Ocean Sci. Discuss., 12, 1893–1912, 2015
www.ocean-sci-discuss.net/12/1893/2015/
doi:10.5194/osd-12-1893-2015

Ocean Science
Discussions
Open Access

A semi-analytical model for diffuse reflectance in marine and inland waters

J. D. Pravin[1], P. Shanmugam[1,2], and Y.-H. Ahn[2]

[1]Ocean Optics and Imaging Laboratory, Department of Ocean Engineering, Indian Institute of Technology Madras, Chennai, 600036, India
[2]Korea Ocean Satellite Research Center, KIOST, Seoul 425-600, Korea

Received: 15 June 2015 – Accepted: 22 July 2015 – Published: 19 August 2015

Correspondence to: P. Shanmugam (pshanmugam@iitm.ac.in)

Published by Copernicus Publications on behalf of the European Geosciences Union.

Abstract

A semi-analytical model for predicting diffuse reflectance of coastal and oceanic waters is developed based on the water-column optical properties and illumination conditions. Diffuse reflectance (R) is an apparent optical property that is related to the Gordon's parameter ($b_b/(a+b_b)$) through a proportionality factor "f". The conventional assumption of "f" as a constant (0.33) yields large errors in case of turbid and productive coastal waters and a predictive model based on this assumption is generally restricted to open-ocean waters (low chlorophyll case). In this paper, we have sorted the dependent factors that influence "f" values in the water column. Here, the parameter "f" is modeled as a function of wavelength, depth, inherent optical properties (IOPs) and illumination conditions. This work eliminates the spectral constants (K_{Chl} and K_{SS}) associated with our previous model and constrains the present model to be solely dependent on the IOPs and illumination conditions. Data used for parameterization and validation are obtained from in situ measurements in different waters within coastal environments. Validation shows good agreement between the model R and in situ R values with the overall mean relative error of less than a few percent. The model is valid for a wide range waters within coastal and open-ocean environments.

1 Introduction

The significance of reflectance is generally well-known as it is the main physical quantity that contains the information regarding the seawater constituents such as phytoplankton, suspended sediments, detrital and dissolved organic matter (Mobley, 1994; Thomas and Stamnes, 2002). Reflectance properties of the seawater constituents vary substantially from one water type to another water type, permitting interpretation of their existence, nature and composition. Moreover, it is used to analyze the directional effects (Gordon et al., 1975; Morel and Prieur, 1977), and is a basic quantity used in remote sensing applications. Reflectance is the ratio of incoming and outgoing radiant fluxes and hence it has no unit. It varies between 0 to 1, meaning "0" the complete transmission and "1" the complete reflection. The reflectance values sometimes go beyond 1 only in the case of specular reflecting surfaces and in the case of diffuse (Lambertian) surfaces, values stick equivalent to 1 or even less (Schaepman-Strub et al., 2006). For natural waters, R values can reach up to at the level of 0.4 (for hypereutrophic waters). Any contributions from the bottom (floor) or seagrass can enhance the reflectance considerably. The reflectance spectra are dependent on the inherent optical properties of the seawater but their prediction is very complex. In remote sensing applications, optical properties of the seawater constituents are derived from the reflectance values through inversion models and remote sensing algorithms (Roesler and Perry, 1995; Roesler and Boss, 2003; Shanmugam et al., 2010, 2011; Werdell et al., 2013). Since the reflectance is related to IOPs, the inversion and remote sensing techniques could produce reliable results only if the function "f" is determined accurately.

Determination of exact R is not easy (Mobley, 2005), as the factor f is not a quantity measured directly with a measuring instrument. The prediction of f is complicated as it depends upon many physical and environmental/illumination conditions (Dev and Shanmugam, 2014b). Several researchers have attempted to sort the dependencies of "f" in case 1 waters (Gordon et al., 1975; Morel and Gentili, 1993; Morel and Prieur, 1977). The behavior of f in turbid and productive case 2 waters is difficult to predict, and there is no appropriate and general model reported in the literature. Albert and Mobley developed an analytical model to predict R based on the Hydrolight simulations that is limited in case 2 waters (Albert and Mobley, 2003). Though some of the previously published papers show the dependencies of f on solar angle (Kirk, 1984), wind speed (Albert and Mobley, 2003) and IOPs (Hirata and Højerslev, 2008; Loisel and Morel, 2001; Morel and Gentili, 1993; Sathyendranath and Platt, 1997), they do not include a variety of water conditions within coastal and oceanic environments. Moreover, models accounting the depth-wise variation of R are scarce (Hirata, 2003; Maritorena et al., 1994). Recently, a realistic model of f was reported for a variety of water types and operates as a function of the solar zenith angle, IOPs and wavelength-dependent constants (k_{Chl} and k_{SS}) (Dev and Shanmugam, 2014b). In the present paper, drawbacks of the existing models that were developed based on radiative transfer simulations are overcome by the present model, which is solely dependent on the IOPs and illumination conditions to predict R in coastal and oceanic waters. The wavelength-dependent constants associated with our previous model are eliminated by the measured quantities (particularly the IOPs) and hence more accurate R values are achieved without relying on any assumptions and wavelength-dependent constants.

2 In-situ data

In-situ data were collected on several field campaigns in oceanic and turbid productive coastal waters during May 2012 (Off Point Calimere), August 2013 (Off Chennai), October 2013 (around Chennai coast), November 2013 (Chennai Harbour), May and November 2013 (Muttukaadu lagoon) (Fig. 1). The above field locations are optically different regions characterized by waters with a different composition. Bio-optical measurements were performed on different coastal research vessels (CRV *Sagar Pachimi*, CRV *Sagar Purvi* and BTV *Sagar Manjusha*) allotted by the National Institute of Ocean Technology (NIOT). The radiometric measurements included upwelling and downwelling irradiances from TriOS radiometers and the photometric measurements included absorption and backscattering coefficients from AC-S and BB9 respectively (Dev and Shanmugam, 2014a, b). Chlorophyll fluorescence and turbidity were measured with a FLNTU sensor. Other ancillary data such as temperature, salinity and conductivity were measured by a CTD sensor.

The nature of water is broadly categorized into five types (based on chlorophyll and turbidity levels as schematically shown in Dev and Shanmugam, 2014b): (i) Type I – Clear water (Off Chennai) (Chl $< 1\,\mathrm{mg\,m^{-3}}$ and turbidity < 1 NTU), (ii) Type II – Relatively clear water (around Chennai) ($1 <$ Chl $< 3\,\mathrm{mg\,m^{-3}}$ and $1 <$ turbidity < 3 NTU), (iii) Type III – Relatively turbid water (Chennai Harbour) ($5 <$ Chl $< 25\,\mathrm{mg\,m^{-3}}$ and $1 <$ turbidity < 3 NTU), (iv) Type IV – Turbid water (Off Point Calimere) ($1 <$ Chl $< 3\,\mathrm{mg\,m^{-3}}$

and $3 < \text{turbidity} < 14$ NTU) and (v) Type V – Productive (eutrophic) water (Muttukaadu lagoon) (Chl $> 25\,\text{mg}\,\text{m}^{-3}$ and turbidity > 5 NTU). Further details on the data acquisition and processing protocols as well as methods for laboratory determination of the water constituents can be found elsewhere (Dev and Shanmugam, 2014a, b; Gokul et al., 2014; Simon and Shanmugam, 2013; Sundarabalan and Shanmugam, 2015).

3 Model description

Theoretically, diffuse reflectance (R) is regarded as an apparent optical property (AOP), which is the ratio of upwelling and downwelling irradiances (Eq. 1). In the field of marine optics and remote sensing, it can be calculated analytically from the inherent optical properties (IOP) of the seawater (Eq. 2 or 3).

$$R(0^-,\lambda) = \frac{E_\text{u}(0^-,\lambda)}{E_\text{d}(0^-,\lambda)} \tag{1}$$

$$R(0^-,\lambda) = f(0^-,\lambda)\left(\frac{b_b}{a+b_b}\right) \tag{2}$$

$$R(\lambda,z) = f(\lambda,z)\left(\frac{b_b}{a+b_b}\right) \tag{3}$$

Here R is related to the IOPs through a factor "f" (Gordon et al., 1975; Morel and Prieur, 1977). a and b_b denote the absorption and backscattering coefficients respectively, λ the wavelength, 0^- the depth just below the sea surface, and z the depth layer from the surface. In the literature, the factor f is generally parameterized based on the assumptions related to clear oceanic waters and holds very little information of the other water types in turbid and productive coastal waters. This limits the possibility of extending such models to predict R in coastal oceanic waters. In this paper, f is determined just below the water surface and at different depth levels. As the factor f is dependent partly on the illumination and environmental conditions, analytic solutions for f predictions are not possible (Morel and Gentili, 1991, 1993, 1996). Models with restricted assumptions (such as spectrally invariant, optically homogeneous, zenith sun angle) lower the accuracy of f and hence degrade the predicted reflectance values (Sathyendranath and Platt, 1997). However, based on the experiments conducted in different waters we could provide meaningful interpretation about this complex f factor.

The spectral variation of f is found to have dependency (Loisel and Morel, 2001) on absorption and backscattering coefficients (Eq. 4), whereas its magnitude ($S_f + I_f$) is dependent on the light field available just below the sea level. The entire factor f $(0^-, \lambda)$ seems to follow a power law where its magnitude is the sum of the solar zenith angle function (S_f) and IOP function (I_f). Plotting the $S_f + I_f$ vs. solar zenith angle (Fig. 2a), the data points seem scattered when they are shown together for all water conditions. However, it can be closely observed that the trend followed by each water type is rather consistent although being shifted relative to each other (i.e., Type I (blue) and II (purple) lie at the top, Type III (orange) and IV (pink) in the middle, and Type V (green) at the bottom). Segregating the magnitude term ($S_f + I_f$) provides an insight into the variation of each function with the solar zenith angle (Fig. 2b and c). The term other than the solar zenith angle function (S_f) that seems to influence the f factor is dependent on the IOPs (I_f). We found the relation between this term (I_f) and the inverse of absorption $1/a(400)$ based on the interpretation of reflectance properties of different waters. The model requires four inputs namely the solar zenith angle, Chl concentration, absorption and backscattering coefficients. The model equation is expressed as follows,

$$f(0^-, \lambda) = (S_f + I_f) \cdot \left(\frac{b_b}{a}\right)^n \tag{4}$$

$$f(0^-, \lambda) = \left\{0.03 \cdot \exp^{(0.0462 \cdot \theta_s)} + 0.0684 \cdot \left(\frac{1}{a(400)}\right)^{0.757}\right\} \times \left(\frac{b_b}{a}\right)^n \tag{5}$$

where, $n = 0.03 \times \log(\mathrm{Chl}) + 0.2243$. (6)

As shown mathematically in Eq. (5) and schematically in Fig. 2b and c, S_f increases exponentially with the increase of solar zenith angle and I_f follows a power function which decreases with increasing $a(400\,\text{nm})$. The absorption coefficient at 400 nm is chosen because significant variations in the absorption spectra are evident within this spectral region, whereas at higher wavelengths the absorption due to the pure seawater dominates. Consequently both the S_f and I_f terms determine the magnitude of $f(0^-,\lambda)$.

Conversely, the term "backscattering by absorption ratio" ($b_b a^{-1}$) gives the spectral character to $f(0^-,\lambda)$. The spectral slope is governed by the parameter "*n*", a function of Chl (Fig. 2d) (Okami et al., 1982). In case of clear oceanic waters, the spectral slope "*n*" is small and thereby produces almost linear $f(0^-,\lambda)$. For productive waters with elevated Chl concentrations, the slope causes large spectral variations in $f(0^-,\lambda)$ (Eq. 6). For clear waters (assuming $\text{Chl} = 0.1\,\text{mg}\,\text{m}^{-3}$), it takes the value of 0.194 and for turbid productive waters ($\text{Chl} = 72\,\text{mg}\,\text{m}^{-3}$), it takes the value of 0.28 (note that Chl values presented in this paper refer to FLNTU-measured Chl). Considering all the water types, the predicted $S_f + I_f$ values are in excellent agreement with in situ $S_f + I_f$ determinations (Fig. 2e).

The depth wise f function $[f(\lambda,z)]$ is largely dependent on the f just below the surface $[f(0^-,\lambda)]$. As noted earlier, the $f(0^-,\lambda)$ is a function of light field available at just below the water surface which is approximated on the basis of the solar zenith function and IOPs. The relation between light fields just beneath the air–water interface (0^-) and the depth z is given by,

$$f(\lambda,z) = f(0^-,\lambda) \times e^{-z(K_\text{u}-K_\text{d})} \tag{7}$$

$$R(\lambda,z) = f(\lambda,z)\left(\frac{b_b}{a+b_b}\right)$$

$$R(\lambda,z) = f(0^-,\lambda)\left(\frac{b_b}{a+b_b}\right) \times e^{-(K_\text{u}-K_\text{d})z} \tag{8}$$

where $f\ (0^{-},\lambda)$ is from Eq. (5). In case, if the oceanic system is homogeneous, R throughout the water column must be uniform without any fluctuations. This in turn sheds light on the f function of both 0^{-} and z. For the uniform R throughout the vertical column, $R\ (0^{-},\lambda)$ must be equivalent to $R(\lambda,z)$. Since most of the natural waters are non-homogeneous (because the water constituents are in general not homogeneously distributed) the fluctuations of R are expected. The fluctuations in R are replicated on the f. Since f is a function of light field available in the water column, it tends to decrease with depth as denoted by $-z$ (minus z) in Eq. (7). The term $(K_\mathrm{u}-K_\mathrm{d})$ is the change in the upwelling and downwelling diffuse attenuation coefficients that induce the corresponding change (increase or decrease) in $f(\lambda,z)$. Thus, any underwater fluctuations in R depend on the change in the upwelling and downwelling diffuse attenuation coefficients (Eqs. 7 and 8).

4 Results and discussion

For evaluating the performance of the present model, the underwater diffuse reflectance profiles for the considered five water bodies were modeled based on the measured IOPs (absorption and backscattering) and the derived $f(\lambda,z)$ and $(K_\mathrm{u}-K_\mathrm{d})$ values. The model R values were then compared with those determined from in situ measurements of upwelling and downwelling irradiances. Figure 3a$_1$–e$_2$ shows the comparison of model-derived and measured reflectances for each water types (Type-I to Type-V), wherein the black line represents the measured R and the orange line represents the simulated R. Two examples from each water type are presented (in column wise). The sub-plots labeled as a, b, c, d and e correspond to the water Types I to V respectively and the subscripts 1 and 2 represent two different stations for a particular water type. The R spectra of each water type (ranging from clear to turbid) are unique and distinct from each other in its spectral shape. Figure 3a$_1$ and a$_2$ represents the clear oceanic Type-I waters with very low chlorophyll concentration ($< 0.25\,\mathrm{mg\,m^{-3}}$) and low turbidity ($< 0.6$ NTU). The presence of very low seawater contents diminishes the absorption coefficient in the blue region that subsequently gives high reflectance in this spectral region. At higher wavelengths, high absorption and low backscattering produce very low reflectance tending close to zero. The model is able to produce the *R* spectra similar to the in situ *R* spectra. Figure 3b_1 and b_2 represents the relatively clear Type-II waters with Chl concentration and turbidity less than 2 mg m^{-3} and 2 NTU. Here, the absorption coefficient is comparatively higher than that of Type-I waters that diminishes the magnitude of the reflectance in the blue region. This is clearly seen with the primary peak shifting from the blue region (Type 1 case) to the green region (around 500–550 nm) due to the absorption effect. Though the Chl concentration at these stations is greater than 1 mg m^{-3}, the secondary peak (around 685 nm) is not well pronounced due to the considerable amount of suspended sediments (that increased turbidity level from 1.4–2 NTU). The considerable amount of suspended sediments enhances backscattering at higher wavelengths (650–700 nm), resulting in non-zero reflectance spectra. The reflectance spectra predicted by the model agree well with the in situ measurements.

In Type-III waters with Chl nearly five times greater than its turbidity level, chlorophyll (and of course, other constituents such as colored dissolved substance and non-algal particles) absorbs light strongly in the blue portion, further diminishing the reflectance spectra below 0.01 (Fig. 3c_1 and c_2). The reflectance spectra predicted by the model are consistent with the in situ spectra, wherein both the primary and secondary peaks are well pronounced because of the elevated Chl concentration and reduced turbidity.

The Type-IV waters are dominated by suspended sediments and little chlorophyll in contrast to the Type-III waters. The turbidity level at these two stations (Fig. 3d_1 and d_2) is greater than 5 NTU, while the Chl concentration remains low ($< 2\,\mathrm{mg\,m^{-3}}$). At these stations, high backscattering by suspended sediment particles is particularly effected in the NIR region and hence the enhanced *R* values when compared to the previous cases (Types I, II and III). As a consequence, the secondary peak around 685 nm is suppressed because of the elevated suspended sediment concentration relative to the Chl concentration. The absorption effect of algal and non-algal particles is seen as the reduced R in the blue part of the spectrum. The model remains stable and consistent in terms of reproducing the measured R spectra.

The applicability of this model is also verified in turbid productive (eutrophic) waters characterized by very high turbidity (> 7 NTU) and Chl ($44\,\mathrm{mg\,m^{-3}}$). The typical R spectra from these waters are shown in Fig. 3e_1 and e_2, wherein the primary peak is further shifted toward the yellow spectral region and the secondary peak toward the NIR region. The combined effect of both backscattering and fluorescence/absorption tends to cause a reflectance peak at NIR (Ahn and Shanmugam, 2007; Dev and Shanmugam, 2014a; Shanmugam et al., 2013). The absorption by phytoplankton, non-algal particles and dissolved substance is abnormally high so that the R values approach near-zero (< 0.005) in the blue region. Notably, the predicted R spectra agree well with the measured R spectra despite the slight discrepancy in the red portion.

The consistency of the model to predict the vertical profiles of reflectance is further investigated. Figure 4a and b displays the variation of R throughout the water column. For brevity, the results are shown only for two stations – one from turbid coastal water off Point Calimere (Fig. 4a) and the other from Chennai Harbour water (Fig. 4b). Two examples are chosen randomly to show the closeness of the model results with measurements. Since the water constituents are not homogeneously distributed with depth in these water bodies, R cannot be constant throughout the water column and can either increase or decrease vertically depending on the constituents present in it (Hirata, 2003). Fluctuations in $R(\lambda, z)$ can be accurately predicted by the exponential term "$K_u - K_d$" in Eq. (8). If $K_u > K_d$, R decreases and if $K_u < K_d$, R increases. This behavior of R has been discussed in Dev and Shanmugam (2014b). As shown in Fig. 5, the agreement between the model and measured R values is generally good in each case and they consistently acknowledge the increasing and decreasing trends throughout the water column. These results confirm that the model is capable of accurately predicting spectral and vertical distributions of R in different waters within coastal environments.

Further statistical analysis performed on the spectral and vertical R profile data from the model and measurements (Table 1) demonstrates significantly lower errors (RMSE

$\leq 21.4\,\%$; MRE ≤ 5.8; Bias ≤ 0.053) and higher slope and R^2 values. The one-to-one correspondence with small errors across the entire visible region and depth levels confirms the validity of the present model in a wide range of conditions within coastal environments.

Comparing the present model with existing models, it should be noted that the existing are designed with certain assumptions to predict R in case 1 waters or coastal (case 2) waters. For instance, a model that is originally developed for clear oceanic case 1 waters (Gordon et al., 1975; Morel and Prieur, 1977; Kirk, 1984) gives biased reflectance values in turbid coastal and productive water types. A model of case 2 waters (Albert and Mobley, 2003) is found restricted to case 2 waters (Dev and Shanmugam, 2014b). In contrast, the present model is purely based on the analytical and experimental results, and is well suited for a wide range of waters within open-ocean and coastal environments. The inter-comparison of the results from this model and existing models is not shown in this work for brevity.

5 Conclusion

A semi-analytical model has been developed to predict the spectral and vertical profiles of diffuse reflectance in coastal oceanic waters. The model results were validated with measurement data from a wide variety of coastal and open ocean waters. The model proves to be efficient in terms of reproducing these in situ data from five water types with the desired accuracy. This model overcomes the limitations associated with existing models and predicts R as a function of IOPs and illumination conditions. The present model is applicable to homogenous, inhomogeneous as well as stratified waters. It is anticipated that it will have great significance in hydrologic optics, remote sensing studies, underwater imaging and related engineering applications.

Acknowledgement. This research was supported by INCOIS under the grant (OEC1314117INCOPSHA) of the SATCORE program. The work was partly supported by the Korea Ocean Satellite Centre, Korea Institute of Ocean Science and Technology

(KIOST) through support from the Korean Federation of Science and Technology Societies (KOFST), Korea. We would like to thank D. Rajasekhar, The Head, Vessel Management Cell (VMC), and Director of National Institute of Ocean Technology (NIOT) for providing the CRV *Sagar Purvi*, CRV *Sagar Pachimi* and BTV *Sagar Manjusha* (Coastal Research Vessels) to Indian Institute of Technology (IIT) Madras, Chennai, India. We are thankful to the Topical Editor, Mario Hoppema, for providing valuable comments to improve the quality of this manuscript.

References

Ahn, Y.-H. and Shanmugam, P.: Derivation and analysis of the fluorescence algorithms to estimate phytoplankton pigment concentrations in optically complex coastal waters, J. Opt. A-Pure Appl. Op., 9, 352–362, doi:10.1088/1464-4258/9/4/008, 2007.

Albert, A. and Mobley, C. D.: An analytical model for subsurface irradiance and remote sensing reflectance in deep and shallow case-2 waters, Opt. Express, 11, 2873–2890, doi:10.1364/OE.11.002873, 2003.

Dev, P. J. and Shanmugam, P.: A new theory and its application to remove the effect of surface-reflected light in above-surface radiance data from clear and turbid waters, J. Quant. Spectrosc. Ra., 142, 75–92, doi:10.1016/j.jqsrt.2014.03.021, 2014a.

Dev, P. J. and Shanmugam, P.: New model for subsurface irradiance reflectance in clear and turbid waters, Opt. Express, 22, 9548–9566, doi:10.1364/OE.22.009548, 2014b.

Gokul, E. A., Shanmugam, P., Sundarabalan, B., Sahay, A., and Chauhan, P.: Modelling the inherent optical properties and estimating the constituents' concentrations in turbid and eutrophic waters, Cont. Shelf Res., 84, 120–138, doi:10.1016/j.csr.2014.05.013, 2014.

Gordon, H. R., Brown, O. B., and Jacobs, M. M.: Computed relationships between the inherent and apparent optical properties of a flat homogeneous ocean, Appl. Opt., 14, 417–27, 1975.

Hirata, T.: Irradiance inversion theory to retrieve volume scattering function of seawater, Appl. Opt., 42, 1564–73, 2003.

Hirata, T. and Højerslev, N. K.: Relationship between the irradiance reflectance and inherent optical properties of seawater, J. Geophys. Res., 113, C03030, doi:10.1029/2007JC004325, 2008.

Kirk, J. T. O.: Dependence of relationship between inherent and apparent optical properties of water on solar altitude, Limnol. Oceanogr., 29, 350–356, doi:10.4319/lo.1984.29.2.0350, 1984.

Loisel, H. and Morel, A.: Non-isotropy of the upward radiance field in typical coastal (Case 2) waters, Int. J. Remote Sens., 22, 275–295, 2001.

Maritorena, S., Morel, A., and Gentili, B.: Diffuse reflectance of oceanic shallow waters: influence of water depth and bottom albedo, Limnol. Oceanogr., 39, 1689–1703, doi:10.4319/lo.1994.39.7.1689, 1994.

Mobley, C. D.: Light and Water: Radiative Transfer in Natural Waters, Academic Press, Inc., San Diego, 1994.

Mobley, C. D.: Informal Notes on Reflectances, Sequoia Scientific, Inc, Bellevue, WA 98005, 2005.

Morel, A. and Gentili, B.: Diffuse reflectance of oceanic waters: its dependence on Sun angle as influenced by the molecular scattering contribution, Appl. Opt., 30, 4427–4438, 1991.

Morel, A. and Gentili, B.: Diffuse reflectance of oceanic waters. II. Bidirectional aspects, Appl. Opt., 32, 6864–6879, 1993.

Morel, A. and Gentili, B.: Diffuse reflectance of oceanic waters. III. Implication of bidirectionality for the remote-sensing problem, Appl. Opt., 35, 4850–4862, 1996.

Morel, A. and Prieur, L.: Analysis of variations in ocean color, Limnol. Oceanogr., 22, 709–722, doi:10.4319/lo.1977.22.4.0709, 1977.

Okami, N., Kishino, M., Sugihara, S., and Unoki, S.: Analysis of ocean color spectra (I) – calculation of irradiance reflectance, J. Oceanogr. Soc. Japan, 38, 208–214, 1982.

Roesler, C. S. and Boss, E.: Spectral beam attenuation coefficient retrieved from ocean color inversion, Geophys. Res. Lett., 30, 1468, doi:10.1029/2002GL016185, 2003.

Roesler, C. S. and Perry, M. J.: In situ phytoplankton absorption, fluorescence emission, and particulate backscattering spectra determined from reflectance, J. Geophys. Res., 100, 13279–13294, doi:10.1029/95JC02176, 1995.

Sathyendranath, S. and Platt, T.: Analytic model of ocean color, Appl. Opt., 36, 2620–2629, 1997.

Schaepman-Strub, G., Schaepman, M. E., Painter, T. H., Dangel, S., and Martonchik, J. V.: Reflectance quantities in optical remote sensing – definitions and case studies, Remote Sens. Environ., 103, 27–42, doi:10.1016/j.rse.2006.03.002, 2006.

Shanmugam, P., Ahn, Y.-H., Ryu, J.-H., and Sundarabalan, B.: An evaluation of inversion models for retrieval of inherent optical properties from ocean color in coastal and open sea waters around Korea, J. Oceanogr., 66, 815–830, 2010.

Shanmugam, P., Sundarabalan, B., Ahn, Y.-H., and Ryu, J.-H.: A New Inversion Model to Retrieve the Particulate Backscattering in Coastal/Ocean Waters, IEEE T. Geosci. Remote, 49, 2463–2475, doi:10.1109/TGRS.2010.2103947, 2011.

Shanmugam, P., Suresh, M., and Sundarabalan, B.: OSABT: An innovative algorithm to detect and characterize ocean surface algal blooms, IEEE J. Sel. Top. Appl., 6, 1879–1892, 2013.

Simon, A. and Shanmugam, P.: A new model for the vertical spectral diffuse attenuation coefficient of downwelling irradiance in turbid coastal waters: validation with in situ measurements, Opt. Express, 21, 30082, doi:10.1364/OE.21.030082, 2013.

Sundarabalan, B. and Shanmugam, P.: Modelling of underwater light fields in turbid and eutrophic waters: application and validation with experimental data, Ocean Sci., 11, 33–52, doi:10.5194/os-11-33-2015, 2015.

Thomas, G. E. and Stamnes, K.: Radiative Transfer in the Atmosphere and Ocean, Cambridge University Press, 73–77, 2002.

Werdell, P. J., Franz, B. A., Bailey, S. W., Feldman, G. C., Boss, E., Brando, V. E., Dowell, M., Hirata, T., Lavender, S. J., Lee, Z., Loisel, H., Maritorena, S., Mélin, F., Moore, T. S., Smyth, T. J., Antoine, D., Devred, E., d'Andon, O. H. F., and Mangin, A.: Generalized ocean color inversion model for retrieving marine inherent optical properties, Appl. Opt., 52, 2019–2037, doi:10.1364/AO.52.002019, 2013.

Table 1. Statistical comparison of the model and in situ R for five types of waters.

λ	RMSE	MRE	Bias	Slope	Intercept	R^2
412	0.214	−0.012	−0.024	0.772	−0.466	0.829
448	0.185	−0.018	−0.033	0.851	−0.305	0.86
488	0.17	−0.022	−0.038	0.908	−0.188	0.839
531	0.154	−0.02	−0.03	0.928	−0.139	0.777
555	0.148	−0.018	−0.027	0.922	−0.14	0.755
670	0.181	−0.025	−0.053	0.955	−0.144	0.849
685	0.214	−0.058	−0.121	1.023	−0.075	0.846
710	0.197	−0.006	−0.013	0.995	−0.024	0.897

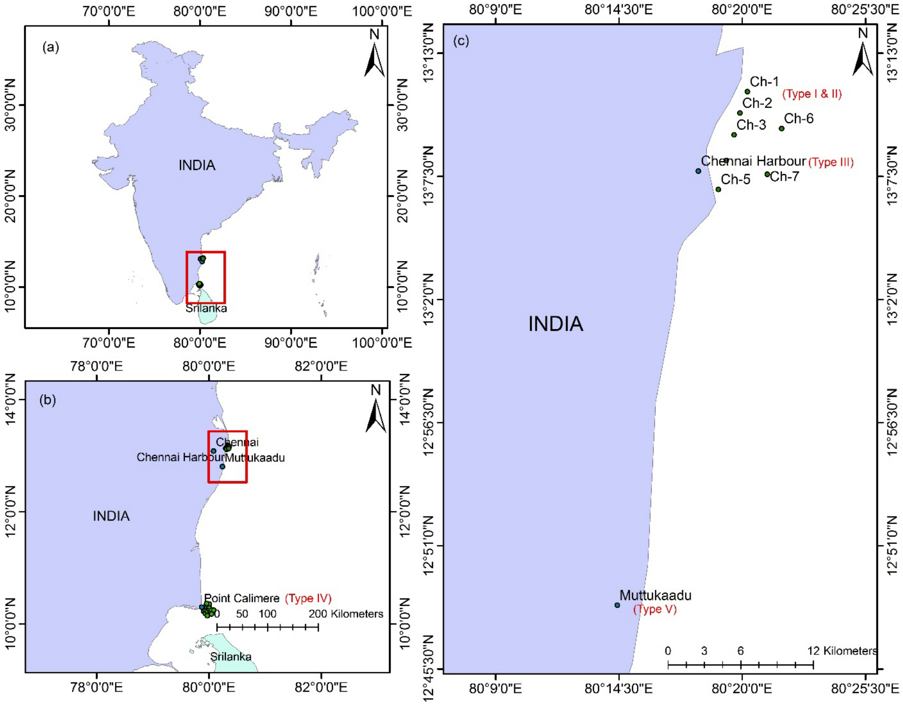

Figure 1. (a) Study sites on the southeast part of India (shown in red box). **(b)** Magnified study area covering Chennai, Muttukadu and Point Calimere. **(c)** Magnified study area with stations covering Chennai (Type I, II, and III) and productive Muttukaadu lagoon system (Type V).

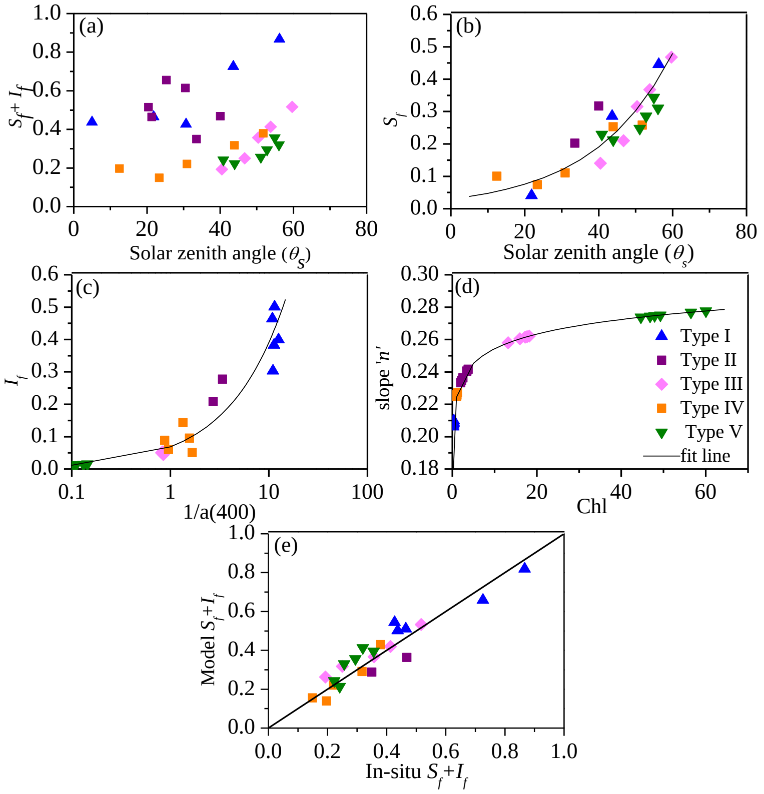

Figure 2. Scatter plots showing dependencies of (**a** and **b**) S_f on the solar zenith angle, **(c)** I_f on the $1/a(400)$, **(d)** Chl on the spectral slope parameter "n" and **(e)** 1 : 1 correspondence of model and in situ S_f and I_f.

Title Page
Abstract | Introduction
Conclusions | References
Tables | Figures
◀▎ | ▶▎
◀ | ▶
Back | Close
Full Screen / Esc

Printer-friendly Version
Interactive Discussion

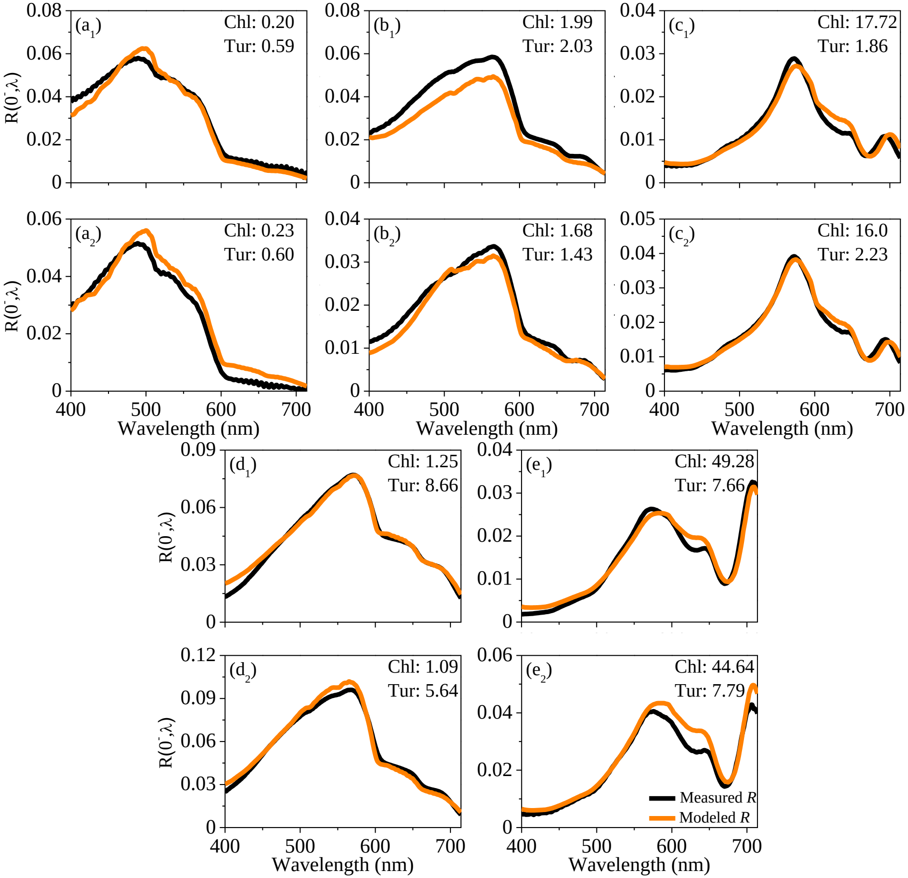

Figure 3. Comparison of the modeled *R* (orange line) and measured *R* (black line) from different waters.

Title Page
Abstract
Introduction
Conclusions
References
Tables
Figures
|◀
▶|
◀
▶
Back
Close
Full Screen / Esc
Printer-friendly Version
Interactive Discussion

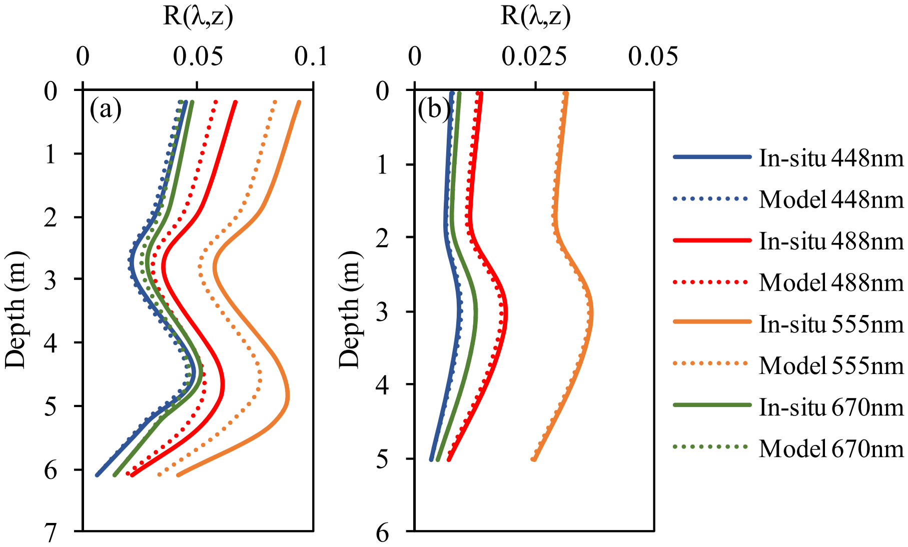

Figure 4. Vertical profiles of the modeled and measured *R* from for two coastal waters sites (results shown for some key wavelengths). Bold lines represent the measured *R* and the dotted lines represent the model *R*.

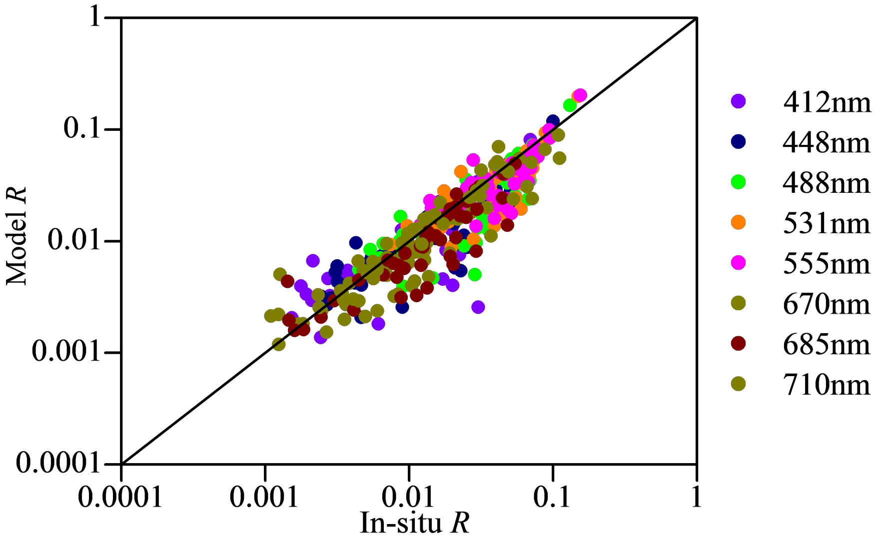

Figure 5. Scatter plots comparing the model R and in situ R from all five types of waters and depth levels (results shown for some key wavelengths: 412, 448, 488, 531, 555, 670, 685 and 710 nm).